Applied Catalysis B: Environmental 99 (2010) 118–126

Contents lists available at ScienceDirect

Applied Catalysis B: Environmental

journal homepage: www.elsevier.com/locate/apcatb

A comparative study of $Ba_{0.5}Sr_{0.5}Co_{0.8}Fe_{0.2}O_x$ (BSCF) and $SrFeCo_{0.5}O_x$ (SFC) ceramic membranes used for syngas production

Sedigheh Faraji, Karen J. Nordheden, Susan M. Stagg-Williams*

Chemical and Petroleum Engineering Department, The University of Kansas, USA

ARTICLE INFO

Article history:
Received 31 December 2009
Received in revised form 30 March 2010
Accepted 7 June 2010
Available online 11 June 2010

Keywords:
Ceramic membrane
BSCF
SFC
$Pt/CeZrO_2$
Pt/ZrO_2
Syngas production

ABSTRACT

Dense oxygen permeable ceramic membranes are promising materials for separating oxygen from air and for syngas production. In this work, the role of two different membrane materials, $Ba_{0.5}Sr_{0.5}Co_{0.8}Fe_{0.2}O_x$ (BSCF) and $SrFeCo_{0.5}O_x$ (SFC), in the conversion of methane, has been studied. Pulse and temperature programmed desorption studies of CO and CO_2 showed a higher CO and CO_2 adsorption on BSCF compared to the SFC membrane. More CO adsorption resulted in more CO_2 production. Raman spectroscopy of BSCF and SFC ceramic materials after CO and CO_2 exposure showed carbonate species on these samples. Both H_2 and O_2 adsorption were significantly higher on BSCF, with significant water formation in the presence of hydrogen. Reaction investigations over Pt-based catalysts demonstrated higher methane conversion and a higher H_2:CO ratio on the BSCF membrane than on the lower flux SFC membrane because of more interaction of the products with BSCF. Under reaction conditions, the simultaneous occurrence of steam and CO_2 reforming of methane would lead to a higher methane conversion and a higher H_2:CO ratio on BSCF. The onset temperature of oxygen release for BSCF was observed to be lower than that for SFC while the amount of oxygen release was significantly greater. These studies suggest that BSCF might be suitable for hydrocarbon conversion reactions at much lower temperatures than conventional dense ceramic membranes.

1. Introduction

Using non-porous oxygen-conducting ceramic membranes has received significant attention over the past few decades as an environmentally benign process for production of either syngas ($CO + H_2$) or hydrogen. These oxygen permeable ceramic membranes behave as alternatives to the conventional expensive syngas production process based on an air separation plant. The interest in such selective ceramic membranes is due to their intrinsic ability to act as oxygen suppliers or oxygen distributors at high temperatures in the oxidation process of methane [1–3] or other hydrocarbons [4,5]. Ceramic membranes, which are made of metal oxides, can be classified into two types: cobalt-based membranes and cobalt-free membranes. It is believed that cobalt-based membranes like $SrFeCo_{0.5}O_x$ (SFC) and $Ba_{0.5}Sr_{0.5}Co_{0.8}Fe_{0.2}O_x$ (BSCF) have high oxygen flux but low stability which leads to membrane failure during long-term operation, while the opposite is true about cobalt-free membranes [6]. A great deal of research has been done on using dense SFC and BSCF ceramic membranes for methane conversion to syngas [7–10]. BSCF has also been introduced as a high-performance solid oxide fuel cell (SOFC) cathode material in the literature [11,12].

We have previously shown that when a disk-shaped SFC ceramic membrane is used in conjunction with an unreduced Pt/ZrO_2 catalyst, the oxygen from the ceramic membrane is more beneficial to the methane conversion than the co-fed oxygen [13]. Also, we have shown that there is a synergistic relationship between a $Pt/CeZrO_2$ catalyst and a SFC ceramic membrane. The synergistic relationship results in the production of water and the subsequent occurrence of steam and CO_2 reforming of methane leads to higher methane formation when the catalyst and the ceramic membrane are in close contact under reaction condition [14]. In our previous flux studies on ceramic membranes, dense BSCF membranes, which have a higher mechanical stability than SFC, demonstrated 10 times higher oxygen permeation flux than dense SFC membrane at 800 °C [15]. These dense BSCF membranes maintain long-term mechanical integrity and stability in an air:Ar gradient at 800 °C and the membrane oxygen flux (0.57 sccm/cm^2) at this condition is consistent with other literature studies [16,17].

The goal of this study is to compare the performance of dense BSCF membranes with that of dense SFC ceramic membranes for converting CH_4 to syngas in the presence of $Pt/CeZrO_2$ and Pt/ZrO_2

* Corresponding author at: Chemical and Petroleum Engineering Department, University of Kansas, 1530 W, 15th Street, 4132 Learned Hall, University of Kansas, Lawrence, KS 66045, USA. Tel.: +1 785 864 2919; fax: +1 785 864 4967.
E-mail address: smwilliams@ku.edu (S.M. Stagg-Williams).

0926-3373/$ – see front matter © 2010 Elsevier B.V. All rights reserved.
doi:10.1016/j.apcatb.2010.06.008

catalysts. Specific emphasis will be placed on the surface reactions and reaction mechanisms. The role of the membrane material in the enhancement of methane conversion is investigated by studying the adsorption and desorption of reactant and product species. We explore how the partial substitution of Sr with Ba affects the interaction of ceramic material with O_2, H_2, CO, and CO_2, and how it influences product distribution and H_2/CO ratio during CO_2 reforming of methane.

2. Experimental

2.1. Ceramic membranes preparation

SFC powder (Praxair Specialty Ceramics) was passed through a 60-mesh sieve and coated with 1 wt% ethylcellulose binder prior to pressing. The SFC powder was then pressed at a pressure of 60 MPa for 3 min and sintered at 1180 °C in flowing air for 10 h (heating rate: 1.2 °C/min). During the sintering procedure, the binder burns off between 350 °C and 450 °C. The presence of the binder did not affect the density of the finished SFC membranes, which is approximately 94% of the theoretical density.

A citrate–EDTA method was used to prepare the BSCF powder [18]. First, stoichiometric amounts of Ba, Sr, Co, and Fe nitrate were added into EDTA–$NH_3{\cdot}H_2O$ solution, to which citric acid was added. The molar ratio of total metal ion:EDTA:citric acid was 1:1:1.5. The pH of the solution was adjusted to 6 by adding $NH_3{\cdot}H_2O$. With heating and stirring, a dark purple gel was formed. The gel was heated and dried in air at 110–120 °C and a powder was obtained. The powder was calcined at 950 °C for 5.5 h in a muffle furnace to obtain the BSCF powder. The BSCF powder was then pressed in the stainless steel die (2 cm diameter) under 250 MPa for 5 min. Finally, the membrane was sintered at 1100 °C for 5 h with ramping and cooling rate of 1 °C/min in the muffle furnace.

The surface of the final disk-shaped membranes required substantial grinding and polishing with a combination of aluminum oxide abrasive film and a lathe to ensure adequate sealing in the membrane reactor. The thickness of both membranes was approximately 2 mm after polishing. The fluxes of the SFC and BSCF membranes in an air:Ar gradient were measured at 0.05 sccm/cm^2 and 0.57 sccm/cm^2, respectively.

For pulse studies in plug flow reactor and also thermogravimetric analysis (TGA) and Raman studies, the prepared disk-shaped SFC and BSCF membranes were subsequently crushed and then passed through a sieve to obtain a particle size smaller than 250 μm. This procedure ensures that the SFC and BSCF pieces used for the above studies have the same composition and state as the disk-shaped membranes.

2.2. Catalyst preparation and characterization

Pt/$CeZrO_2$ and Pt/ZrO_2 were prepared by depositing Pt on commercially available ZrO_2 and $CeZrO_2$ support material (MEL CHEM, with 18 wt% of Ce) using the incipient wetness impregnation technique with an aqueous solution of $H_2PtCl_6{\cdot}6H_2O$. Prior to deposition, the substrates were calcined at 800 °C. After deposition, the material was dried overnight at 120 °C and then calcined at 400 °C for 2 h in flowing air (30 cm^3/min). The catalysts were not reduced prior to the experiments in this study.

The percentage of Pt on the Pt/ZrO_2 and Pt/$CeZrO_2$ catalyst was determined by ICP analysis (Galbraith Laboratories) and the results showed 0.404 wt% and 0.50 wt% Pt in the Pt/$CeZrO_2$ and Pt/ZrO_2 catalysts, respectively. TEM images of fresh samples of the catalysts showed that the Pt was highly dispersed on the catalyst support. This analysis was performed at the Microscopy Laboratory at the University of Kansas on a FEI High Resolution Transmission Electron Microscope (TECNAI F20 X-Twin).

2.3. Raman spectroscopy

A Raman spectrometer was used to provide molecular-level information about adsorbed CO and CO_2 species on the fresh ceramic membranes under different reaction conditions. A SENTERRA Dispersive Raman Spectrometer (BRUKER), which is equipped with a CCD camera and located at the University of Kansas, was employed to collect the Raman spectra for each ceramic material in the spectral range of 80–2630 cm^{-1}. The Raman spectra using a 785 nm excitation laser (10 mW power) were recorded at a resolution of 3–5 cm^{-1}. A 50× objective was used to focus on the sample surface. He, CO, and CO_2 gases were introduced to the samples, which were placed into the sample stage (Linkam, FTIR 600) at different temperatures. The sample stage was capable of raising the temperature up to 600 °C. The desired flow rate of each gas was maintained within an FMA-5876A OMEGA flow controller.

2.4. Thermogravimetric analysis (TGA)

TGA was performed on samples to determine changes in mass and heat flow in relation to change in temperature. This analysis was performed on a DSC-TGA (TA Q600) (capable of reaching 1500 °C) at the University of Kansas. Almost 90 mg of each crushed membrane was placed into a clean alumina pan and heated to 800 °C in nitrogen (100 ml/min) and also in air (20 ml/min) at a heating rate of 3 °C/min.

2.5. Reaction tests

The pulse studies and temperature programmed desorption (TPD) experiments on the crushed membranes were performed in a 6 mm i.d. quartz tube plug flow reactor at atmospheric pressure. The reactor temperature was controlled by a temperature controller (Omega; CN 3000). A total of 10–20 mg of the crushed membrane was loaded into the reactor for each test. For pulse studies, the reactor was heated to 800 °C with an argon-only feed (15 ml/min) and then held at this temperature. 50 μl pulses of H_2, O_2, CO, and CO_2 (10 ml/min of each) were injected into the reactor until no changes were observed. For the TPD tests, the reactor was heated to 800 °C in Ar (15 ml/min) after the sample was exposed to a 30-min continuous flow of CO or CO_2 at room temperature. The reactor then was held at 800 °C until all adsorbates were removed from sample surface. The reactor effluent composition was quantified using a Balzers OmniStar mass spectrometer. In addition, the inlet flow rate was monitored continuously using an Agilent ADM2000 flow meter. Quantification of the species in the effluent was performed using calibration injections of known mixtures.

Reaction tests over dense disk-shaped ceramic membranes were conducted in a two-sided concentric quartz tube reactor as shown in Fig. 1. 10 mg of a supported platinum catalyst powder was spread evenly in a thin layer (~1 mm) across the entire portion of the membrane surface. This small quantity of catalyst minimizes transport limitations within the catalyst layer and ensures good proximity between the membrane material and the entire catalyst bed. The whole reactor was put into a tubular electrical furnace and a K-type thermocouple was used to control the temperature of the furnace (heating and cooling rates: 1 °C/min). The reactor was sealed at 800 °C using gold ring seals between the outer quartz tubes and the membrane surfaces. An external pneumatic press maintained pressure against the gold seal. 130 ml/min air was introduced into the bottom side of reactor (oxygen supply side of the membrane), and 20 ml/min argon was used to sweep the

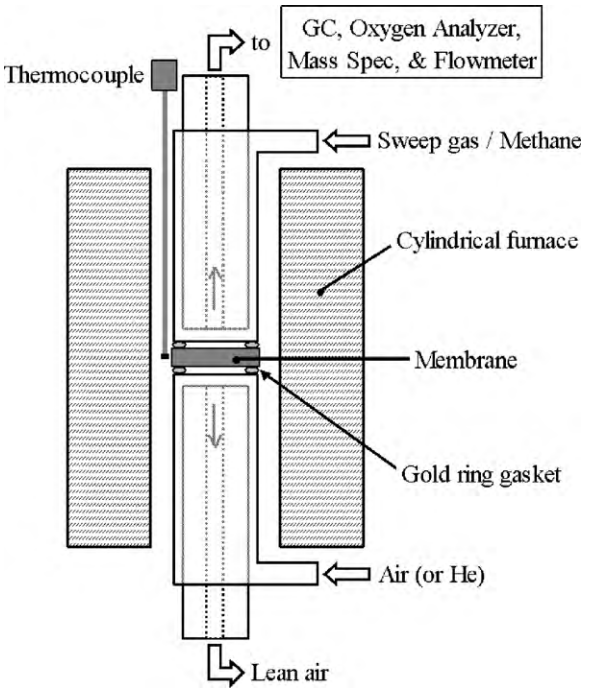

Fig. 1. Membrane reactor schematic.

top side of reactor (oxygen permeate side of the membrane). The effluent of the oxygen-lean side of the membrane was analyzed simultaneously with the Balzers Omnistar mass spectrometer and a SRI 8610C gas chromatograph. The GC was equipped with a Supelco Carboxen 1010 PLOT column. A CH_4:CO_2 volumetric ratio of 1:1 was used in all tests with 20 mol% argon comprising the remainder of the feed stream. The feed flow rate was 25 ml/min, which corresponds to a modified space velocity of 150 l/h/$g_{catalyst}$. In addition to the ceramic membranes, a stainless steel "blank" membrane painted with an inert BN_3 paint to prevent reaction on the steel surface, was used as an inert control to provide baseline data for the ceramic membrane experiments. For all reaction tests, effluent water was calculated from a hydrogen atom balance and the resulting trends were confirmed with mass spectrometer data. For each run, the material balance closed within approximately 2%.

3. Results and discussion

3.1. O_2 uptake and release capability of SFC and BSCF

Ceramic materials can reduce or oxidize reaction species because of their oxygen uptake and release capability, leading to a change in overall reaction mechanism. Thus, it is important to understand the interaction of oxygen with the BSCF and SFC membrane materials. For this purpose, each crushed ceramic material was loaded into a plug flow reactor and was heated to 800 °C in argon. Fig. 2A shows mass spectrometer oxygen signal for both materials while heating in argon. The onset temperature of oxygen release for BSCF (almost 450 °C) was observed to be lower than that for SFC, while the total amount of oxygen release was greater for BSCF (1.87e−6 mol for BSCF vs. 4e−7 mol for SFC). SFC started to release oxygen at 550 °C and it did not show a significant oxygen release before this temperature. Fig. 2A suggests that BSCF might be suitable for hydrocarbon conversion reactions at much lower temperatures than conventional dense ceramic membranes. It is worth mentioning that a similar oxygen release experiment was performed in membrane reactor for disk-shaped BSCF and SFC membranes. The dense ceramic membranes were heated to 800 °C

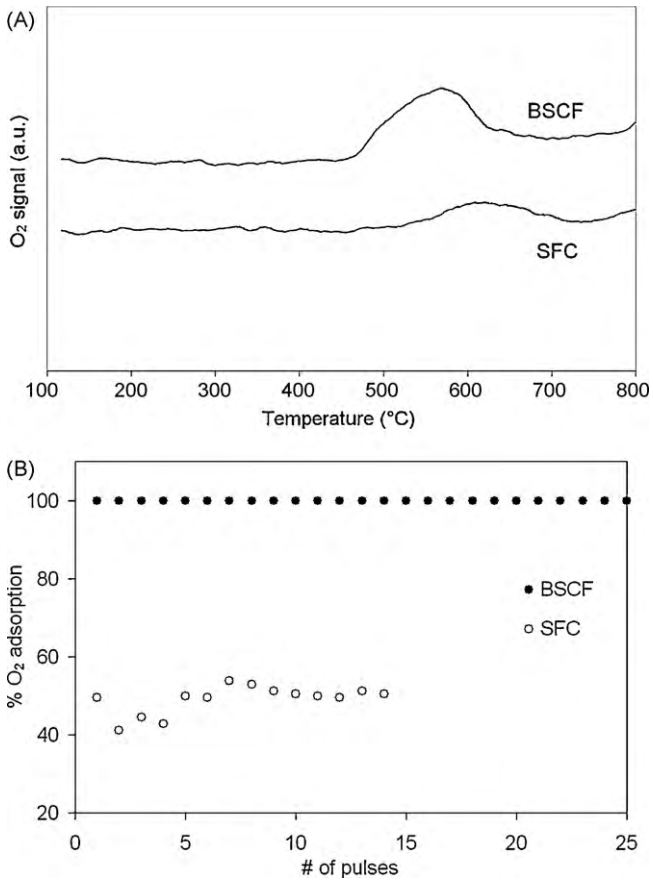

Fig. 2. Oxygen interaction with crushed SFC and BSCF in plug flow reactor: (A) thermal O_2 release in Ar and (B) O_2 uptake during pulses of oxygen at 800 °C and atmospheric pressure.

in flowing argon, while the effluent oxygen signal was monitoring by mass spectrometer. The results in membrane reactor were similar to those in plug flow reactor (i.e., low-temperature oxygen release was greater for BSCF).

At 800 °C, the crushed SFC and BSCF samples were exposed to 50 μl O_2 injections and both samples showed oxygen adsorption capability. However, according to Fig. 2B, the amount of oxygen uptake on BSCF was significantly higher than that on SFC. For the crushed BSCF membrane, no oxygen peak was observed in mass spectrometer even 3 h after the first oxygen injection, indicating that all of the oxygen was adsorbed by the BSCF. These results clearly show the higher adsorption capacity of the BSCF membranes compared to SFC.

TGA studies were used to clarify the mass changes of crushed ceramic materials in different atmospheres (air and nitrogen) from room temperature to 800 °C. The results of the TGA studies are shown in Fig. 3. During the heating process in N_2, both SFC and BSCF undergo weight loss due to their oxygen release capabilities. However, the amount of weight loss in BSCF specimen is higher than that in SFC specimen. This observation is consistent with Fig. 2A in which the total amount of oxygen release in argon was greater for BSCF. The calculated amount of weight loss for BSCF in N_2 is almost 0.0064 mg/mg BSCF. Based on Fig. 2A, 92% of this weight loss is due to oxygen release and the remainder is probably due to water and other surface contaminants. It is interesting to note that the samples behave differently in air, where oxygen is available to replenish oxygen lost. According to Fig. 3, at temperatures ranging from 400 °C to 500 °C in flowing air, BSCF shows a large weight loss while SFC gains weight. This means that at this temperature range, BSCF can release oxygen even in an oxygen-rich atmosphere, but

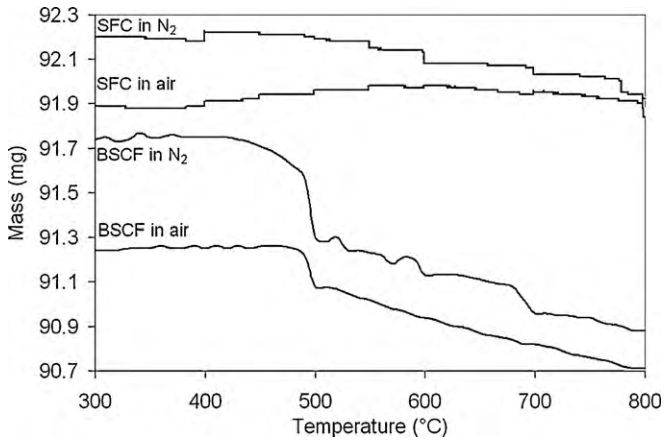

Fig. 3. TGA profiles for crushed SFC and BSCF in flowing nitrogen and air.

SFC tends to adsorb oxygen in such an atmosphere. Over this temperature range, the drop in weight for BSCF in air is smaller than that in nitrogen, which is to be expected due to the difference in the equilibrium oxygen content of the membrane in the different environments. At temperatures above 600 °C, SFC shows a weight loss similar to BSCF. These TGA studies again suggest that BSCF may be a suitable material for reactions occurring at low temperatures specifically between 400 °C and 500 °C.

During another TGA test (data not shown), a continuous flow of air was introduced to crushed BSCF and SFC samples at 800 °C, after being heated in flowing nitrogen to 800 °C. The results show that samples gain weight upon exposure to air. However, the amount of mass increase, which represents the amount of oxygen uptake, for BSCF particles is 2.5 times higher than that for SFC particles. This observation is in agreement with what was observed in plug flow reactor during 50 μl O_2 injections at 800 °C (Fig. 2B).

3.2. H_2, CO, and CO_2 interaction with SFC and BSCF

The primary products formed from the decomposition of methane in the presence of CO_2 (dry reforming) or O_2 (partial oxidation) are H_2 and CO. Previous studies have suggested that the hydrogen formed during the reaction can interact with oxygen species on the membrane surface to form water [13]. In addition, it has been suggested that CO_2 and CO can form carbonate species on the membrane surface [11,12,19–21]. For BSCF, $Sr_{0.6}Ba_{0.4}CO_3$ carbonate has been observed after CO_2 adsorption [21]. The formation of H_2O, and the adsorption and potential reaction of CO and CO_2 on the membrane surface, can significantly change the product composition and the overall reaction scheme. Thus, it is important to understand the interaction of the reactant and product species with the membrane material.

To understand the interaction of ceramic membranes with H_2, CO, and CO_2 at 800 °C, the crushed SFC and BSCF samples were heated to 800 °C in argon in the plug flow reactor. Then, each sample was exposed to 50 μl pulses of H_2, CO, or CO_2 while monitoring the effluent using a mass spectrometer.

During H_2 injections at 800 °C, hydrogen consumption and water production were observed for both the BSCF and SFC crushed samples. Fig. 4 compares the relative amounts of total hydrogen consumption for BSCF and SFC. It is clear from Fig. 4 that the amount of hydrogen consumed for the BSCF was more than 24 times higher than that for SFC. This increased hydrogen consumption resulted in a significant increase in the amount of water produced for BSCF compared to SFC. The consumption of hydrogen and the appearance of water, clearly demonstrates that the both membrane materials have the ability to react with gaseous hydrogen. However, in the absence of an oxygen supply, the crushed SFC membrane material is not able to replenish the oxygen in the lattice, and the hydrogen consumption quickly ceases. For BSCF, lattice oxygen is available for water production even 4 h after first hydrogen injection, again indicating that BSCF is a better oxygen supplier than SFC.

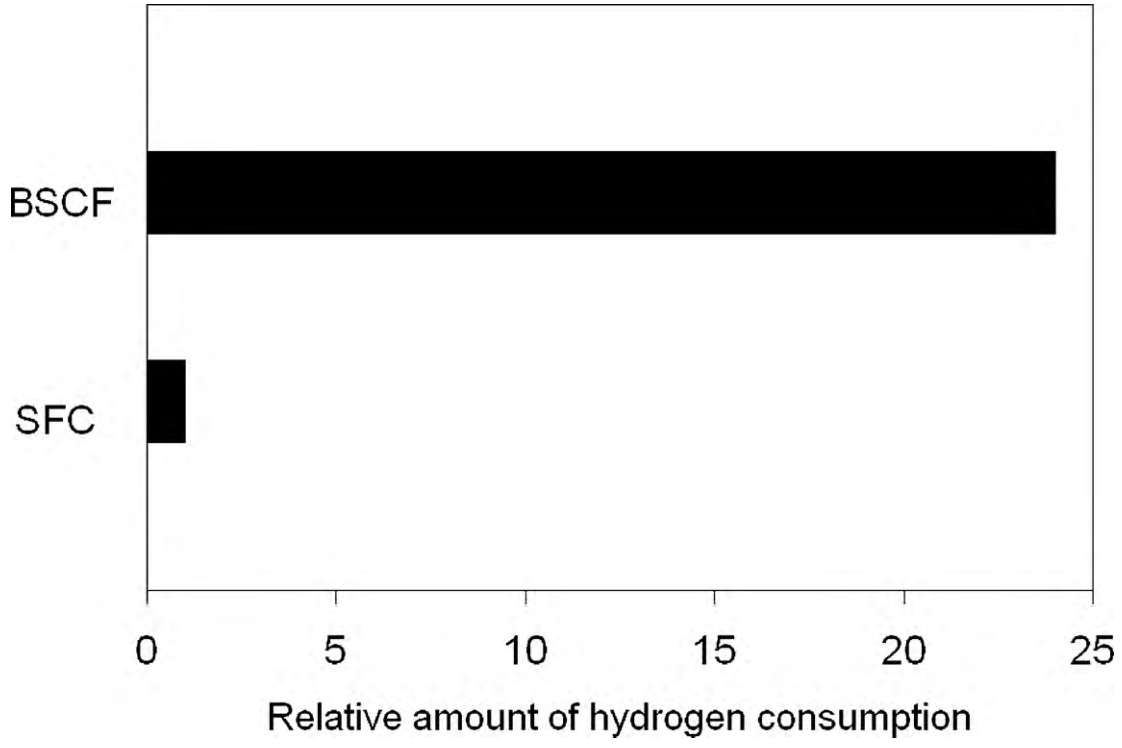

Fig. 4. The relative amount of total hydrogen consumption at 800 °C and atmospheric pressure for crushed BSCF and SFC.

When CO was injected on the BSCF and SFC samples at 800 °C, CO_2 production was seen for both samples. Fig. 5A and B shows the CO consumption and CO_2 production per one mg of ceramic material. The amount of CO consumption and CO_2 production for BSCF were higher than for SFC. Since the only source of oxygen in the reactor is the oxygen in the membrane lattice, the CO_2 production is ascribed to CO reduction of the membrane. The increased production of CO_2 on the BSCF membrane compared to SFC, clearly shows that the BSCF has the ability to provide higher amounts of oxygen under similar reducing environments than the SFC membrane material. When CO_2 was pulsed into reactor over the BSCF and SFC samples at 800 °C, a small amount of CO production was observed for both membranes. However, there was no significant difference between the interaction of CO_2 with BSCF and that with SFC.

Another set of pulse studies was performed at 800 °C in which the samples were exposed to three sets of pulses. The first set of pulses contained H_2. The second set had CO, followed by the third set, which again contained H_2. Fig. 6 shows the results of this pulse study for the crushed BSCF membrane. Similar to the individual pulse studies, during the first set of H_2 pulses, hydrogen consumption was observed. Likewise, CO_2 was produced during the pulses of CO. It should be noted that the amount of CO_2 produced during the CO pulses is less than the amount of CO consumed. These results suggest that some of the CO does not reduce the membrane surface, but instead remains adsorbed on the membrane surface, possibly in the form of carbonates. During the last set of H_2 pulses, less hydrogen consumption was observed compared to the first set of hydrogen pulses. The decrease in hydrogen consumption during the second set of hydrogen pulses is most likely due to the presence of the adsorbed CO species remaining from the CO pulses. While Fig. 6 shows the results for the BSCF, similar results were observed for the SFC membrane material, indicating that CO adsorption, albeit to a lesser extent, can also occur on the SFC.

Another experiment was performed at 800 °C except the order of the pulses was switched. In this experiment, the order of the pulses

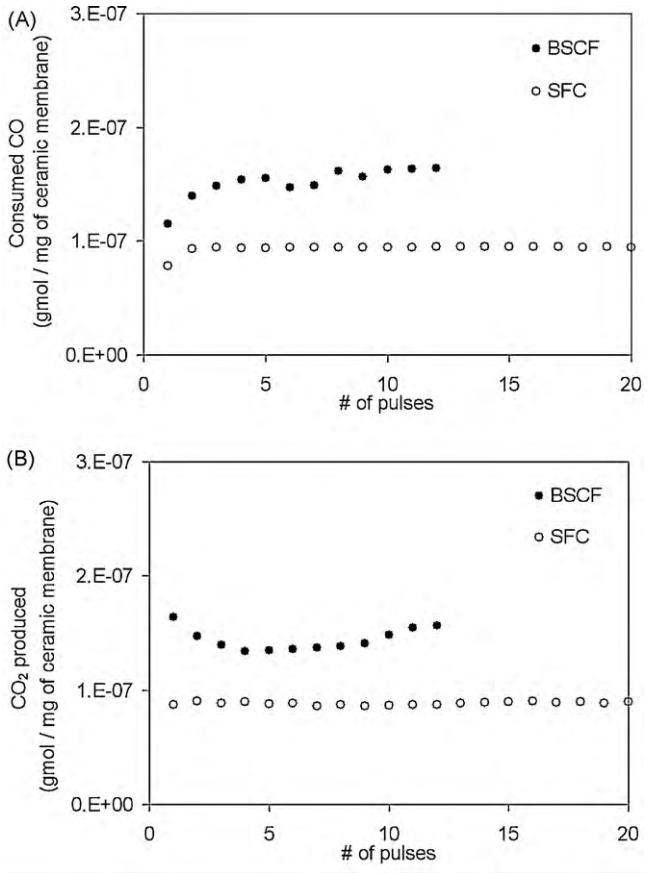

Fig. 5. CO interaction with crushed SFC and BSCF in plug flow reactor at 800 °C and atmospheric pressure: (A) CO consumption profile and (B) CO_2 production profile.

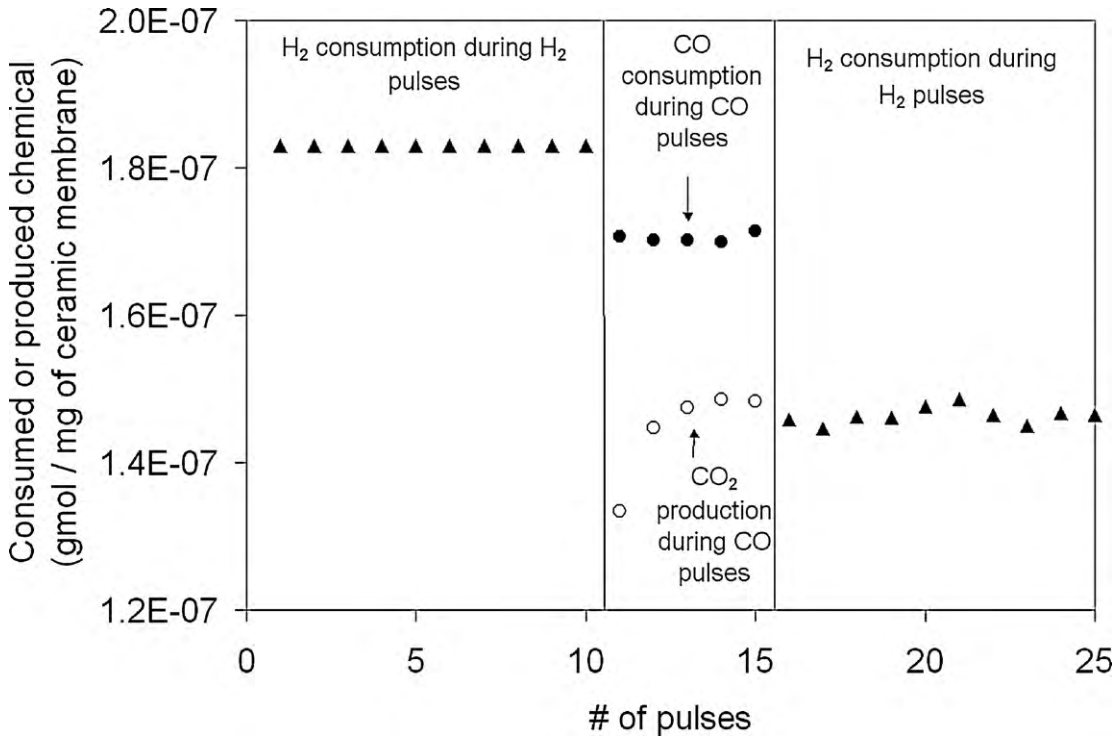

Fig. 6. H_2 and CO interaction with crushed BSCF in plug flow reactor at 800 °C and atmospheric pressure. The order of pulses was H_2/CO/H_2.

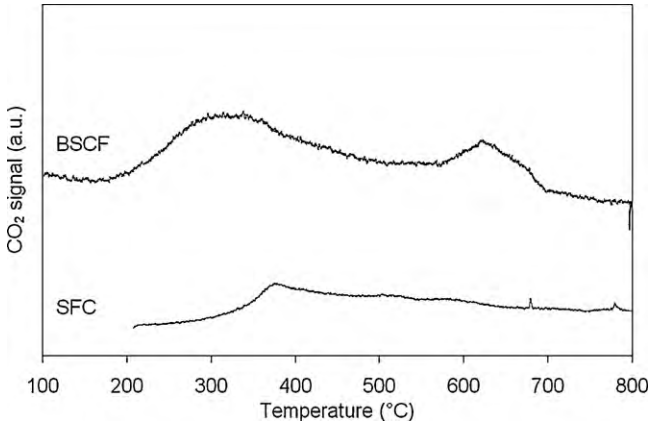

Fig. 7. CO_2 desorption profiles during temperature programmed desorption of CO after exposure to a continuous flow of CO at room temperature.

was $CO/H_2/CO$. Again, CO injections resulted in CO consumption and CO_2 production. However, the CO consumption after hydrogen exposure was higher than that before hydrogen exposure. It is possible that the increase in CO adsorption is due to a hydrogen-assisted adsorption that occurs on the surface of the membrane.

Temperature programmed desorption of CO and CO_2 were performed on each of the samples described above. Each sample was exposed to a continuous flow of CO or CO_2 at room temperature for 30 min and then heated to 800 °C in argon (15 cm^3/min). The effluent was monitored using a mass spectrometer. Figs. 7 and 8 show the CO_2 desorption profiles for the BSCF sample after CO and CO_2 exposure, respectively. Also shown in Figs. 7 and 8 for comparison purposes are the profiles for SFC, under the same conditions, which have been previously reported [14]. In both cases, significant amounts of CO_2 were observed, and no CO was detected. As in the case of the CO pulses at 800 °C, the total amount of CO_2 formed for the BSCF during the TPD of CO and CO_2 is higher than the SFC. It is believed that CO adsorbs to the surface of the ceramic material in the form of carbonates at room temperature but then forms CO_2 at higher temperatures by reducing the material. The onset temperature of CO_2 desorption profile for BSCF sample is 200 °C in Fig. 7 and 250 °C in Fig. 8. Unlike the BSCF, SFC showed a slightly higher onset temperature of CO_2 release. The decreased temperature for CO_2 formation on the BSCF compared to the SFC demonstrates the ability of BSCF to release oxygen more readily than the SFC, and again suggests that BSCF might be a good material for low-temperature reactions.

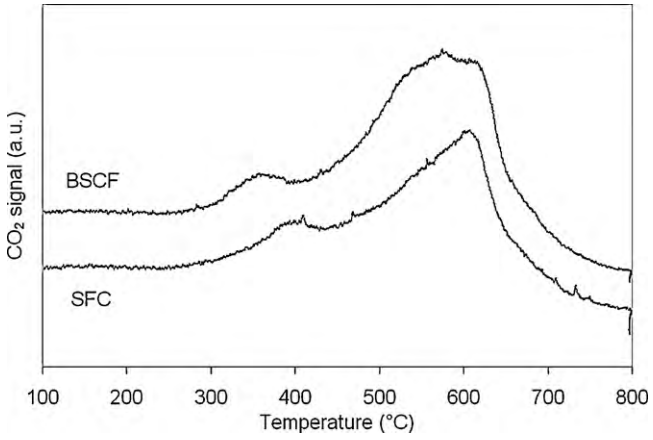

Fig. 8. CO_2 desorption profiles during temperature programmed desorption of CO_2 after exposure to a continuous flow of CO_2 at room temperature.

According to Figs. 7 and 8, two CO_2 desorption peaks were observed for BSCF during heating to 800 °C. It is possible that the two peaks correspond to CO_2 that has been formed from different carbonate species adsorbed on the membrane surface. It is also possible that multiple peaks appear due to different oxygen species (surface versus bulk) contributing to the formation of CO_2. Further studies are needed to differentiate between these possible scenarios.

In order to determine the surface species formed during the ceramic material exposure to CO or CO_2 at different temperatures, samples were scanned by a Raman spectroscope in different flowing gases (He, CO, and CO_2). The results are shown in Figs. 9–12.

The Raman spectra of BSCF and SFC at room temperature in helium are similar; however, the peaks in the spectra of BSCF are slightly shifted to lower wavenumbers. These changes are believed to be due to the presence of Ba in the BSCF sample. The Raman spectra of samples after 30-min exposure to CO and CO_2 at room temperature (Figs. 9 and 10) showed adsorption of these chemicals on the surfaces of BSCF and SFC. Carbonate formation was observed at wavenumber 786 cm^{-1} for BSCF and 787 cm^{-1} for SFC during both exposure to CO and CO_2 [22]. In addition, the band previously assigned to linear CO bonded to the surface was detected at 2056 and 2057 cm^{-1} for BSCF and SFC respectively [23,24]. When CO passes over the sample, it can take oxygen from the surface and form carbonate, which leads to the increase in the band intensity at 786 and 787 cm^{-1}. CO can also attach linearly to the metal atoms on the surface (the band near 2057 cm^{-1}). With exposure to CO_2, dissociation of CO_2 occurs, which results in CO production. Then, this CO can adsorb linearly to the metals on the surface of sample and cause an increase in the intensity of the band at 2057 cm^{-1}. Similarly, the Raman spectra of samples after CO and CO_2 exposure at 400 °C (Figs. 11 and 12) showed CO and CO_2 adsorption on the surfaces of BSCF and SFC. Although it is not possible to obtain the Raman spectra of samples at 800 °C, it is believed that surface species after CO and CO_2 exposure at this temperature are similar to those at room temperature and 400 °C.

It should be noted that no significant changes in the Raman spectra of the samples were observed when the samples were flushed in helium after CO and CO_2 exposure. This indicates that CO and CO_2 are not weakly adsorbed to the ceramic material surfaces.

3.3. *CO_2 reforming of methane in membrane reactor*

The previously described pulse and TPD studies in Sections 3.1 and 3.2 have shown that when SFC and BSCF are exposed to H_2 and CO gases, H_2O and CO_2 formation occur. Also, BSCF has a higher interaction with O_2, H_2, and CO gases compared to SFC, resulting in higher H_2O and CO_2 production. Thus, under reaction conditions and in the presence of a catalyst, hydrogen produced from methane decomposition is expected to result in significant water formation on the BSCF membrane. In addition, both the CO and CO_2 can interact with the membrane surface forming carbonates. The increased water production with the BSCF membranes could lead to more steam reforming occurring in the reactor, effectively increasing the methane conversion. In addition, higher amounts of stream reforming would lead to higher H_2:CO ratios in the reactor effluent due to the 3:1 ratio of H_2:CO for steam reforming compared to the 1:1 H_2:CO ratio expected for CO_2 reforming.

These hypotheses were tested by investigating the CO_2 reforming of CH_4 at 800 °C over Pt/ZrO_2 and $Pt/CeZrO_2$ catalysts on dense BSCF and SFC membranes. To understand the role of the membrane, the reactions were also carried out using the catalysts placed on top of a stainless steel blank coated with an inert BN_3 paint. In the tests with the inert blank, the reaction was not assisted by oxygen since there is no oxygen flux with the stainless steel blank. Figs. 13 and 14 show the methane conversion profile and H_2/CO ratio for the exper-

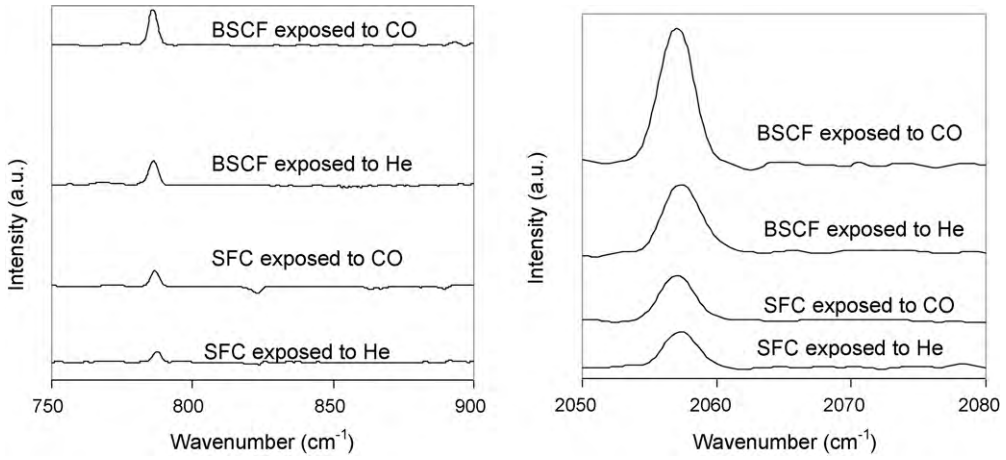

Fig. 9. The Raman spectra of crushed SFC and BSCF at room temperature in flowing CO.

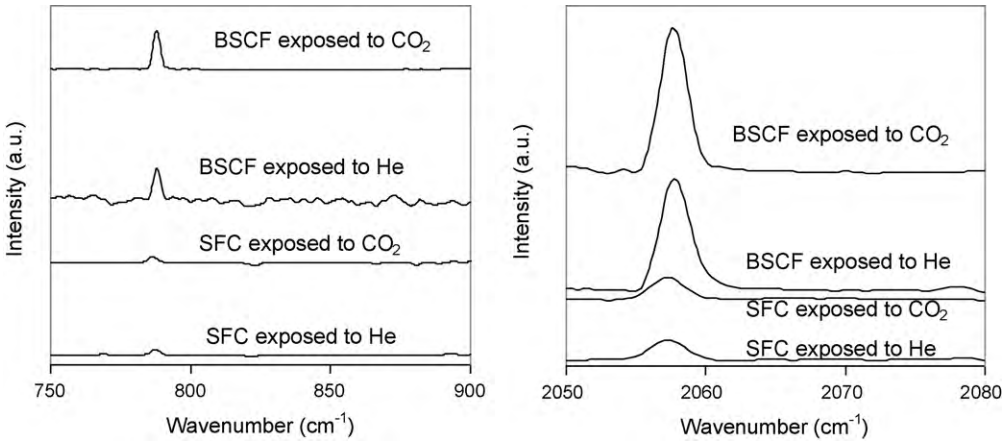

Fig. 10. The Raman spectra of crushed SFC and BSCF at room temperature in flowing CO_2.

iments described above. For all tests, CH_4 conversion and H_2/CO ratio decrease as time proceeds. As is expected, the H_2/CO ratio of $Pt/CeZrO_2$ is higher than that of Pt/ZrO_2 both with and without the ceramic membranes due to the ability of the Ce promoted support to participate in the reaction [25]. Both catalysts show higher H_2/CO ratio in the presence of ceramic membranes than in the presence of stainless steel blank, indicating the beneficial effects of oxygen from ceramic membrane on the reaction. More importantly, the methane conversion and the H_2:CO ratio are both higher on the BSCF membrane than on low-oxygen flux SFC membrane, while the CO_2 conversion is less on BSCF.

The high H_2:CO ratio and low CO_2 conversion on BSCF can be due to increased steam reforming and more CO conversion to CO_2 on the BSCF membrane compared to the SFC membrane. Fig. 15 shows the water production and CO_2 conversion over $Pt/CeZrO_2$ catalyst. Relative water production is high on the BSCF membrane

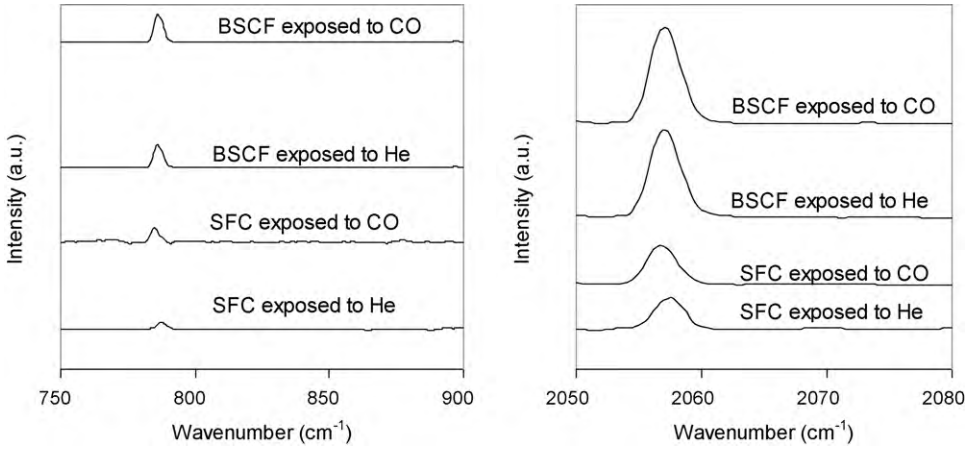

Fig. 11. The Raman spectra of crushed SFC and BSCF at 400 °C in flowing CO.

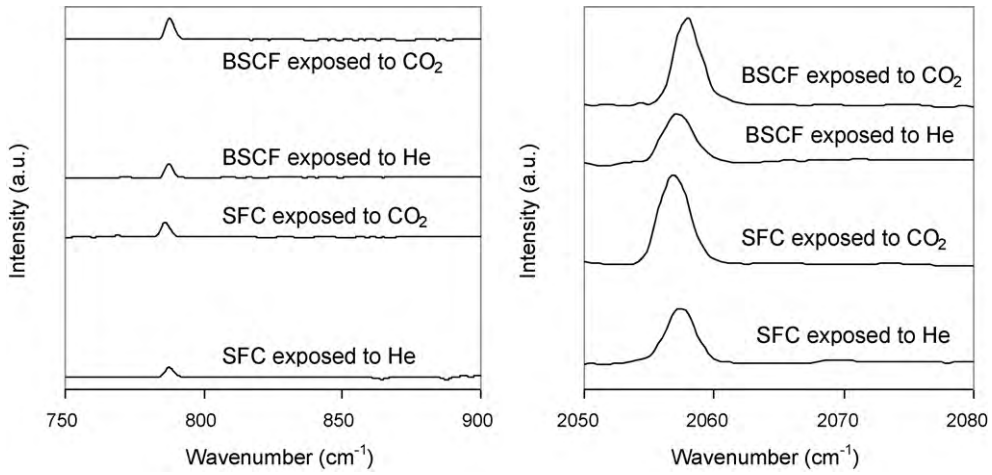

Fig. 12. The Raman spectra of crushed SFC and BSCF at 400 °C in flowing CO_2.

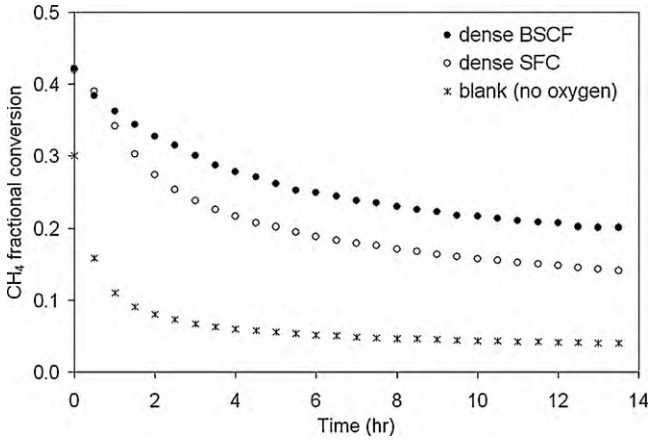

Fig. 13. Methane conversion during CO_2 reforming of methane (1:1 ratio) at 800 °C and atmospheric pressure in a membrane reactor over Pt/ZrO_2 catalyst. Feed composition is: 40% CH_4, 40% CO_2, and 20% argon; space velocity is 150 l/h/$g_{catalyst}$.

with the $Pt/CeZrO_2$ catalyst but not so with the Pt/ZrO_2 catalyst. The low CO_2 conversion and high water production eliminate the possibility of significant reverse water gas shift reaction with the BSCF membrane and the $Pt/CeZrO_2$ catalyst. Combustion is a possible co-reaction with CO_2 reforming on the $Pt/CeZrO_2$ catalyst. Previous studies [26] have suggested that combustion occurs via oxygen diffusion from the membrane to the gas phase, or oxygen spillover directly to the catalyst. Based on the studies in this work, diffusion of molecular oxygen from the membrane surface to the gas phase under reaction conditions seems unlikely. Oxygen spillover from highly reducible supports to metal particles has been shown for many reactions. However, the spillover usually occurs when the metal particle is in intimate contact with the support. In this case, the catalyst is loosely dispersed on the membrane surface, and the spillover would have to occur from the membrane surface to the metal particle via the catalyst support. Thus, while oxygen spillover from the membrane surface to the catalyst is then possible, it would be more probable if the catalyst were directly supported on the membrane surface. It should be noted that the products of combustion, water and CO_2, are the same products that are formed from hydrogen and CO oxidation on the membrane surface. Based on the data from the studies in this work, the most likely explanation for the high H_2:CO ratio, increased CH_4 conversion, and decreased CO_2 conversion observed is the interaction of oxygen species on the membrane surface with H_2 leading to the formation of water. The water can then participate in the reaction via steam reforming. Similarly, for Pt/ZrO_2 catalyst on BSCF, a combination of CO_2 reforming and steam reforming seems most likely. These results are similar to the results obtained previously where asymmetric BSCF showed higher methane conversion and H_2:CO ratio but lower CO_2 conversion than dense SFC for CO_2 reforming of CH_4 [27].

Based on the reaction tests and the surface studies performed a network of possible reactions can occur. CO_2 dissociation to CO and CH_4 decomposition to H_2 are two initial steps of the reaction mechanism when CH_4 and CO_2 are fed into reactor simultaneously.

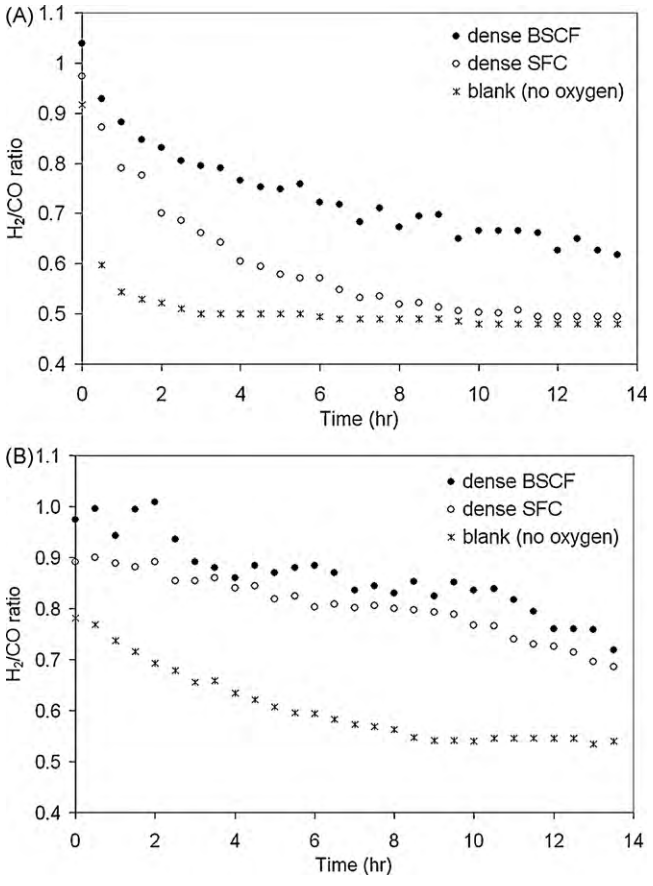

Fig. 14. H_2:CO ratios during CO_2 reforming of methane (1:1 ratio) at 800 °C and atmospheric pressure in a membrane reactor over: (A) Pt/ZrO_2 catalyst and (B) $Pt/CeZrO_2$ catalyst. Feed composition is: 40% CH_4, 40% CO_2, and 20% argon; space velocity is 150 l/h/$g_{catalyst}$.

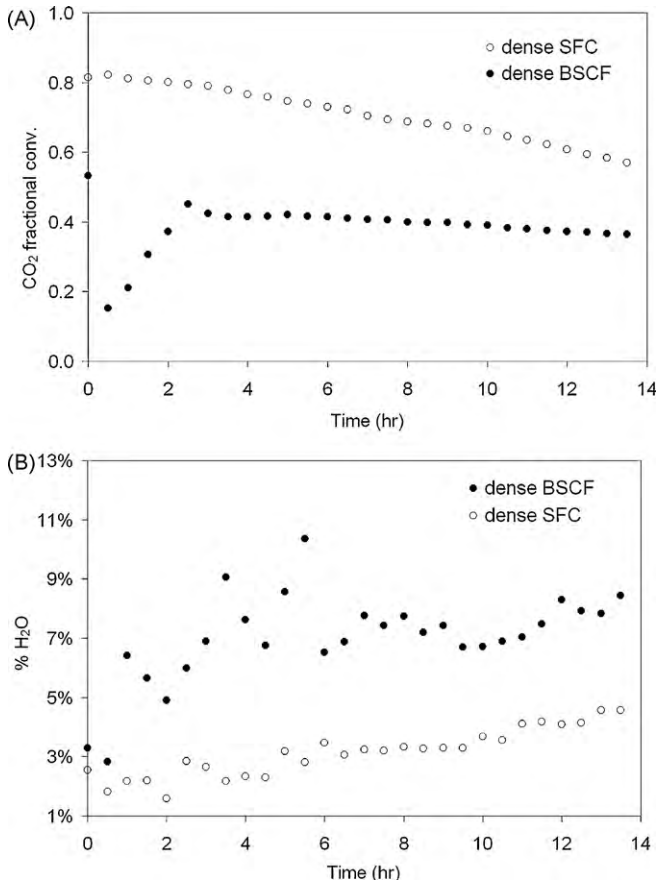

Fig. 15. CO_2 conversion (A) and water production (B) during CO_2 reforming of methane (1:1 ratio) at 800 °C and atmospheric pressure in a membrane reactor over $Pt/CeZrO_2$ catalyst. Feed composition is: 40% CH_4, 40% CO_2, and 20% argon; space velocity is 150 l/h/$g_{catalyst}$.

H_2 and CO are both reducing agents which can reduce the ceramic membrane and produce H_2O and CO_2 (according to Figs. 4 and 5). Water can react with CH_4 and produce more CO and H_2 (steam reforming). Water can also participate in a reaction with CO to produce H_2 and CO_2 (water gas shift). Furthermore, for high oxygen flux membranes, and with intimate contact of the membrane and catalyst, it may be possible that some combustion occurs. Thus, based on the type of catalyst and ceramic membrane used, the extent of each reaction in the above system would vary, resulting in slightly different CH_4 and CO_2 conversions and H_2:CO ratios.

4. Conclusions

Unlike SFC, BSCF exhibited significantly higher O_2 release at low temperatures. This indicates that BSCF could be a promising material for low-temperature oxygen-assisted reactions. BSCF showed higher O_2, H_2, and CO adsorption than SFC. Carbonates were detected on both BSCF and SFC during CO and CO_2 exposure.

The results of CO_2 reforming of CH_4 on dense BSCF and SFC membranes over Pt/ZrO_2 and $Pt/CeZrO_2$ catalysts clearly demonstrated higher methane conversion and H_2:CO ratio on BSCF compared to SFC at 800 °C. The ability of BSCF to adsorb more H_2 and CO than SFC at 800 °C could lead to higher water formation and CO_2 production on this ceramic membrane during CO_2 reforming of methane. The increased formation of H_2O and CO_2 and simultaneous occurrence of steam and CO_2 reforming of CH_4, lead to higher methane conversions and H_2:CO ratio.

Acknowledgments

Financial support for this project was provided by the Office of Naval Research (N00014-03-1-0601) and the US Department of Transportation Research Innovative Technology Administration (DTOS59-06-G-0047). The authors also thank MEL chemicals for providing the catalyst supports.

References

[1] A.J. Jacobson, S. Kim, A. Medina, Y.L. Yang, B. Abeles, Mater. Res. Soc. Symp. Proc. 497 (1998) 29–34.
[2] H.J. Bouwmeester, Catal. Today 82 (2003) 141–150.
[3] C.-Y. Tsai, A.G. Dixon, W.R. Moser, Y.H. Ma, AIChE J. 43 (1997) 2741–2750.
[4] W. Zhu, W. Han, G. Xiong, W. Yang, Catal. Today 104 (2005) 149–153.
[5] W. Zhu, W. Han, G. Xiong, W. Yang, Catal. Today 118 (2006) 39–43.
[6] P. Zeng, Z. Chen, W. Zhou, H. Gu, Z. Shao, S. Liu, J. Membr. Sci. 291 (2007) 148–156.
[7] P.S. Maiya, U. Balachandran, J.T. Dusek, R.L. Mieville, M.S. Kleefisch, C.A. Udovich, Solid State Ionics 99 (1997) 1–7.
[8] B. Ma, N.I. Victory, U. Balachandran, B.J. Mitchell, J.W. Richardson, J. Am. Ceram. Soc. 85 (2002) 2641–2645.
[9] B. Ma, U. Balachandran, Mater. Res. Bull. 33 (1998) 223–236.
[10] J.H. Tong, W.S. Yang, H. Suda, K. Haraya, Catal. Today 118 (2006) 144–150.
[11] Z. Yang, A.S. Harvey, L.J. Gauckler, Scripta Mater. 61 (2009) 1083–1086.
[12] W. Zhou, R. Ran, Z.P. Shao, J. Power Sources 192 (2009) 231–246.
[13] D.A. Slade, A.M. Duncan, K.J. Nordheden, S.M. Stagg-Williams, Green Chem. 9 (2007) 577–581.
[14] S. Faraji, K.J. Nordheden, S.M. Stagg-Williams, Catal. Lett. 131 (2009) 114–121.
[15] Q. Jiang, S. Faraji, D.A. Slade, K.J. Nordheden, S.M. Stagg-Williams, AIChE Annual Meeting Paper no. 509aO, Salt Lake City, 2007.
[16] H. Dong, Z.P. Shao, G.X. Xiong, J.H. Tong, S.S. Sheng, W.S. Yang, Catal. Today 67 (2001) 3–13.
[17] J. Caro, H.H. Wang, C. Tablet, A. Kleinert, A. Feldhoff, T. Schiestel, M. Kilgus, P. Kolsch, S. Werth, Catal. Today 118 (2006) 128–135.
[18] Z.P. Shao, W.S. Yang, Y. Cong, H. Dong, J.H. Tong, G.X. Xiong, J. Membr. Sci. 172 (2000) 177–188.
[19] V. Galvita, L.K. Rihko-Struckmann, K. Sundmacher, J. Mol. Catal. A: Chem. 283 (2008) 43–51.
[20] I. Kaus, K. Wiik, J. Am. Ceram. Soc. 90 (2007) 2226–2230.
[21] A.Y. Yan, L. Bin, Y.L. Dong, Z.J. Tian, D.Z. Wang, M.J. Cheng, Appl. Catal. B: Environ. 80 (2008) 24–31.
[22] C. Li, Y. Sakata, T. Arai, K. Domen, K. Maruya, T. Onishi, J. Chem. Soc. Faraday Trans. I 85 (1989) 929–943.
[23] L.S.F. Feio, C.E. Hori, S. Damyanova, F.B. Noronha, W.H. Cassinelli, C.M.P. Marques, J.M.C. Bueno, Appl. Catal. A: Gen. 316 (2007) 107–116.
[24] A. Davydov, Molecular Spectroscopy of Oxide Catalyst Surfaces, John Wiley & Sons Ltd., Chichester, 2003.
[25] R. Radhakrishnan, R.R. Willigan, Z. Dardas, T.H. Vanderspurt, Appl. Catal. B: Environ. 66 (2006) 23–28.
[26] M. Ikeguchi, T. Mimura, Y. Sekine, E. Kikuchi, M. Matsukata, Appl. Catal. A: Gen. 290 (2005) 212–220.
[27] D.A. Slade, Q. Jiang, K.J. Nordheden, S.M. Stagg-Williams, Catal. Today 148 (2009) 290–297.